

Charge Transfer as a Ubiquitous Mechanism in Determining the Negative Charge at Hydrophobic Interfaces

Emiliano Poli,^{*} Kwang H. Jong, and Ali Hassanali^{*}

*Condensed Matter Statistical Physics Department, The Abdus Salam International Center
for Theoretical Physics, Strada Costiera, Trieste*

E-mail: epoli@ictp.it; ahassanali@ictp.it

Abstract

The origin of the apparent negative charge at hydrophobic-water interfaces has fueled one of the biggest debates in physical chemistry for several decades. The most common interpretation given to explain this observation is that negatively charged hydroxide ions (OH^-) bind strongly to the interfaces. Here, using first principles calculations of the air-water and oil-water interfaces consisting of thousands of atoms, we unravel a mechanism that does not require the presence of OH^- . We show that small amounts of charge transfer along hydrogen bonds and asymmetries in the hydrogen bond network, associated with local topological defects can lead to the accumulation of negative surface charge at both interfaces. For water near oil, we show that there is also some spillage of electron density into the oil leaving it negatively charged. The surface charge densities at both interfaces is computed to be approximately -0.015 e/nm^2 in agreement with electrophoretic experiments. We also show, using an energy decomposition analysis, that the electronic origin of this phenomena is rooted in a collective polarization and charge transfer effect.

Introduction

Air bubbles and oil droplets in water move towards the anode under the presence of electric fields¹⁻³ implying that they develop a natural negative charge. This experimental observation has served as the seed for one of the most hotly debated topics in physical chemistry for the last several decades with numerous conflicting interpretations underlying the origins of the negative charge.⁴⁻⁸ Here we make an important leap in our understanding of this problem providing a framework that helps rationalize the observed phenomena that is rooted in what we propose is a generic charge transfer mechanism associated with the interfacial structure at the surface of water and oil.

The electrokinetic experiments of both air and oil droplets paint a very similar picture despite having rather disparate chemistries namely, that the zeta potential (ζ) vanishes under acidic conditions and that with increasing pH, it becomes increasingly negative showing that these interfaces retain a negative charge at neutral pH.³ If waters constituent ions, the proton and hydroxide are the only sources of charging in water, these experiments suggest that the negatively charged OH^- ions stick to the surfaces with binding energies on the order of 10-20 times larger than thermal energy^{5,6}!

This interpretation has been heavily contested from both experimental and theoretical fronts. Spectroscopy of interfaces using second harmonic generation (SHG) and sum frequency generation (SFG) tell a less consistent picture ranging from the presence of H^+ at the surface under acidic conditions to weak binding of the OH^- under basic conditions.⁹⁻¹³ There have also been other suggestions implicating hydrocarbon impurities such as bi-carbonate ions¹⁴ as the source of the surface charge although this seems to have been ruled out in very recent experimental work interpreting the Jones-Ray effect.¹⁵ Theory and simulations continue to play an important role in the interpretation of these experiments. Several groups have pioneered insightful *ab initio*,¹⁶⁻¹⁸ empirical valence bond¹⁹⁻²¹ and more recently classical empirical potential based²² molecular dynamics simulations of the air-water interface. Most of these studies indicate that the H^+ has some marginal preferential binding to the

surface of water while the OH^- is effectively repelled from this interface.

In this report, we assert that the negative charge at extended hydrophobic interfaces does not require the binding of OH^- ions. Using state-of-the-art linear-scaling density functional theory (LS-DFT) based simulations of thousands of atoms, we elucidate the electronic properties of two paradigmatic systems: the air and oil-water interfaces. Both systems are characterized by a regime of significant negative charge that is primarily modulated by how charge transfer changes for different water defects.²³ Asymmetries in hydrogen bonding patterns between acceptors and donors can cause rather subtle but sizable swings in the charge of water molecules.

At the surface of water, the charge transfer leads to a triple layer of charge with negative surface charge a couple of Angstroms from the surface. While a similar effect occurs at the oil-water interface, an additional complexity emerges: there is some transfer of charge from the water to the oil molecules leaving the latter negatively charged. Interestingly, we show using an energy decomposition analysis that despite the low-dielectric character of the oily molecules, those at the surface experience subtle electronic effects involving both polarization and charge transfer. The surface charge densities that we determine are an order of magnitude larger than those discovered in previous studies^{24–26} bringing them in closer agreement with experiments.

Besides the direct implications in providing fundamentally new insights into the controversy, our results have potential for broader impact. The behavior of hydrophobic interfaces such as the ones we have tackled here, also lie at the heart of fundamental questions in atmospheric²⁷ and pre-biotic chemistry^{28,29} where catalysis plays a critical role. In addition to electrophoretic experiments, there is also a growing literature in the area of triboelectrification, where water near certain hydrophobic interfaces is observed to receive negative charge³⁰ or even a more patchy surface charge distribution at the boundary between different dielectric media.³¹ The electronic and molecular origins of the underlying phenomena in these contexts, remains poorly understood. The charge transfer mechanisms espoused

in this contribution will help broaden the scope of the discussion in the area of contact electrification.

Computational Methods

Most of our results rely on simulations of two different systems that serve as prototypical models for water near hydrophobic surfaces: the surface of water and water near oil. The air-water interface was modeled building a water slab with dimension $40\text{\AA} \times 40\text{\AA} \times 40\text{\AA}$ and adding a vacuum padding of 80\AA on each side of the slab along the z direction. This system comprises of a total of 6540 atoms (2180 water molecules). The second system studied, was a water-oil interface where the oil phase was composed of 200 dodecane molecules, while the water phase was made up of 1960 water molecules leading to a total of 13479 atoms. The cell dimensions for this system are $46.269\text{\AA} \times 46.269\text{\AA} \times 62.768\text{\AA}$.

Our strategy for performing the analysis involved two steps: firstly, classical empirical molecular dynamics simulations were performed in order to allow for large and long-time scale fluctuations that would not be possible using *ab initio* molecular dynamics; secondly, configurations from these simulations were sampled from which the electronic structure calculations were performed. The classical MD simulations were run using the GROMACS software.³² The water phase was modeled using the TIP4P/2005³³ force field in both cases. The dodecane molecules were simulated using the modified OPLS-AA (L-OPLS) potential developed by Böckmann et al.³⁴ This potential has been parametrised on the basis of high level *ab-initio* calculations, densities and heats of vaporization of both short- and long-chain alkanes and on the phase transition temperature of pentadecane in order to extend the OPLS-AA validity to long hydrocarbon chains and recover a more precise description of their phase transition temperatures and ordering.

The air-water system was equilibrated for 10 ns using the NPT ensemble using the Parrinello-Rahaman barostat³⁵ for the first half of the run for bulk water, followed thereafter

by an NVT simulation at 300K opening up a gap in the z-direction which separated the two water surfaces by 160Å for the remainder of the simulation. The production simulations were run for 20 ns. The surface tension computed from the classical simulations is 68.2 in agreement with previous studies.³⁶ From these simulations a total of 250 configurations were randomly selected to perform the electronic structure calculations. The oil-water interfaces were equilibrated first 20 ns via NVT simulations. The production calculations were then run for 40 ns using the isothermal-isobaric ensemble. 200 frames were randomly selected for the electronic structure calculations.

In order to extend the scope of our electronic structure calculations, we employed a Linear Scaling DFT (LS-DFT) approach as implemented in the ONETEP code.³⁷ This technique allowed us to extend the system sizes in our study to thousands of atoms and to model electronic effects of extended hydrophobic interfaces on the nanometer lengthscale. For a more detailed and technical summary of the underlying theory the reader is referred to relevant literature.³⁸ Here we briefly summarize the essential ideas. LS-DFT as implemented in ONETEP makes use of the *nearsightedness*³⁹ inherent to quantum many-body systems by exploiting the single-particle density matrix, $\rho(\mathbf{r}, \mathbf{r}')$ ^{40,41} representation of the system of interest. Within ONETEP, $\rho(\mathbf{r}, \mathbf{r}')$, is expressed in a separable form^{42,43} via atom-centered functions (non-orthogonal generalized Wannier functions, NWGFs⁴⁴), $\phi_\alpha(\mathbf{r})$, as:

$$\rho(\mathbf{r}, \mathbf{r}') = \sum_{\alpha\beta} \phi_\alpha(\mathbf{r}) \mathbf{K}_{\alpha\beta} \phi_\beta^*(\mathbf{r}') \quad (1)$$

In the above, $\mathbf{K}_{\alpha\beta}$ are the matrix elements of the density kernel, which are nonzero only if $|\mathbf{r}_\alpha - \mathbf{r}_\beta| < \mathbf{r}_c$, with \mathbf{r}_α and \mathbf{r}_β representing the coordinates of the centers of ϕ_α and ϕ_β , and \mathbf{r}_c is a real-space cut-off threshold. The truncation of the density kernel ($\mathbf{K}_{\alpha\beta}$) is validated by the exponential decay of $\rho(\mathbf{r}, \mathbf{r}')$ with respect to $|\mathbf{r} - \mathbf{r}'|$ for systems with an electronic band gap.⁴⁵ Such truncation leads to a sparse density matrix ($\rho(\mathbf{r}, \mathbf{r}')$) that makes any insulating or

semi-conducting systems (including the different interfaces considered here) treatable using linear scaling simulation. The NGWFs are centered on the nuclear coordinates and localized within a sphere of radius r_α . Their non-orthogonality, implies a non-diagonal overlap matrix, $S_{\alpha\beta}$:

$$S_{\alpha\beta} = \int d\mathbf{r} \phi_\alpha^*(\mathbf{r}) \phi_\beta(\mathbf{r}) \quad (2)$$

In practice the NGWFs are expressed as a linear combination of coefficients $C_{m\alpha}$, of localized but orthogonal periodic cardinal sine (psinc) functions,⁴⁴ $D_m(\mathbf{r})$, as:

$$\phi_\alpha = \sum_m C_{m\alpha} D_m(\mathbf{r} - \mathbf{r}_m) \quad (3)$$

with m indexing the real-space Cartesian grid inside the spherical localization region of ϕ_α . The psinc functions are obtained from a discrete sum of plane-waves, that makes the set of $D_m(\mathbf{r})$ independent of the nuclear coordinates and systematically improvable upon increase of the kinetic energy cutoff.⁴⁴ The convergence of the ONETEP approach is then dependent on interlinked computational factors such as the kinetic energy cutoff, the number of NGWFs (ϕ_α) per atom and their localization radius.

In our LS-DFT calculations, the adopted kinetic energy cutoff was 1000 eV and 4 NGWFs were used for O atoms and 1 NGWF was used for the H atoms. In all cases, no truncation of the density kernel ($K_{\alpha\beta}$) was enforced. The localization radius for the NGWFs was 10 Bohr in all cases. These parameters were chosen after a careful benchmark for the water monomer and dimer properties against the ab-initio code CP2K.⁴⁶ Simulations were performed using the BLYP^{47,48} functional with Grimmes D2⁴⁹ empirical dispersion corrections. In all cases, separable (Kleinman-Bylander)⁵⁰ norm-conserving pseudopotentials constructed with the Opium code⁵¹ were used.

In order to characterize any possible charge-gradients developing at our simulated interfaces, atomic point charges are then derived from the electron density. The atomic charges reported in this work were calculated using the DDEC3⁵² scheme implementation in ONETEP.⁵³ DDEC3 is an atoms in molecules (AIM) approach where the total QM electron density ($n(r)$) is partitioned into overlapping atomic densities ($n_i(r)$):

$$n_i(r) = \frac{w_i(r)}{\sum_k w_k(r)} n(r) \quad (4)$$

The atomic partial charges are then computed by integrating the atomic electron densities over all space:

$$q_i = z_i - N_i = Z_i - \sum n_i(r) d^3r \quad (5)$$

where N_i is the number of electrons assigned to atom i and z_i is its effective nuclear charge. In the same fashion, higher-order atomic multipoles may be computed as first-order, second-order, (etc) moments of the atomic electron densities. Various definitions of the weighting factors $w_i(r)$ exist. In the DDEC case the weighting function is described so that the atomic weights are simultaneously optimized to resemble the spherical average of $n_i(r)$ and the density of a reference ion of the same element with the same atomic population N_i . In this way, the assigned atomic densities yield a rapidly converging multipole expansion of the QM electrostatic potential and the computed populations are chemically reasonable. A more detailed description of the method can be found in the following references.^{52,53}

An important part of our findings reported in this work is the charge transfer occurring between different types of water molecules at the surface of water and between water and dodecane at the oil-water interface. In particular, the sensitivity of our results to choice of using a standard GGA functional like BLYP was assessed and validated using both hybrid

functionals such as B3LYP⁵⁴ as well as wavefunction approaches such as MP2.⁵⁵ In similar spirit, the charge transfer between water and decane is also found to be generic result with both B3LYP and MP2. Besides the quality of the electronic structure, we also examined the sensitivity of the charge transfer to sampling configurations of the air-water interface sampled from mb-POL⁵⁶ as well using different charge-partitioning schemes. Details of these benchmarks are elucidated in the SI. All in all, we demonstrate that our findings are on firm theoretical footing.

Results and discussion

In the ensuing analysis, we begin by first discussing the charge gradients observed at the surface of water and at the oil-water interface. We subsequently compare and contrast the microscopic origins of the charge oscillations in the two systems.

The Air/Oil Water Interfaces are Negatively Charged

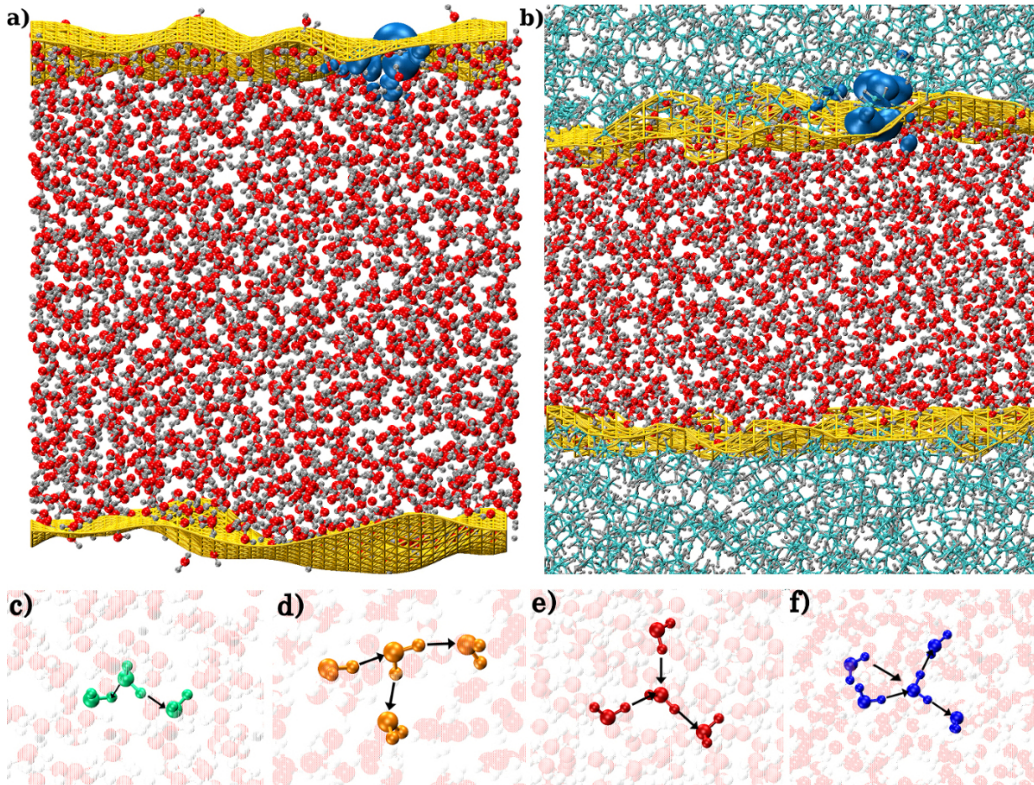


Figure 1: Outline of the two simulated systems: a) the air-water and b) the oil-water. The Willard-Chandler instantaneous surfaces are highlighted in yellow. The Highest Occupied Molecular Orbital (HOMO) in both systems is highlighted in cyan. Panels c), d), e), f) represent the different types of water molecules coordination configurations that will form the focus of our discussion later. For each coordination configuration the accepted hydrogen bond(s) are represented by an arrow pointing in, while the donated hydrogen bond(s) are shown by an arrow pointing out. For brevity, the following nomenclature will be used in the rest of the paper: donated hydrogen bonds will be called *out* while accepted hydrogen bonds will be called *in*. In this way panels c), d), e), f) represent respectively 1in-1out, 1in-2out, 2in-1out and 2in-2out water coordination configurations.

The top left and right panels of Figure 1 show snapshots of our two simulated systems: a) the air-water and b) the oil-water systems consisting of a total of 6540 and 13480 atoms respectively. The yellow-colored surface corresponds to the Willard-Chandler⁵⁷ instantaneous interface (WCI) that is constructed for the water phase. In both figures, the cyan-colored isosurface corresponds to the highest molecular orbital which is localized at the interface. To the best of our knowledge, our simulations represent the first of their kind where the electronic structure of thousands of atoms of the air and oil-water interfaces are treated.

The possibility that a charge transfer mechanism could rationalize the negative charge at hydrophobic surfaces has been suggested in previous theoretical studies^{7,24,25} although the reported charge densities were too small compared to those obtained from electrophoretic experiments. The essential idea is that asymmetries in hydrogen bonding between water molecules at an interface, leads to a subsequent imbalance in the charge transfer along donating versus accepting hydrogen bonds. We begin by showing in Figure 2 the charge densities and integrated surface obtained for the DDEC charges extracted from our calculations for the air-water and oil-water interfaces. As alluded to in Figure 1, in order to perform this analysis, a description of the corrugations of the interface is needed. We used a formulation proposed by Willard and Chandler⁵⁷ which characterizes the instantaneous density fluctuations of the interface. The zero on the x-axes of Figure 2 corresponds to the position of the WCI.

The left panel of Figure 2 reveals the presence of significant charge gradients at the air-water interface covering a length scale of about 5 Å. In particular, we observe a triple layer of charge (green bars): above the instantaneous interface there is a positively charged layer (1st layer) of thickness 1.8Å with a charge density of $\sim 0.0075 \text{ e/nm}^3$; immediately below this, there is a compensating negative layer of similar thickness (2nd layer) but with a larger charge density of $\sim -0.012 \text{ e/nm}^3$; and finally, below 2-5Å from the interface, there is another positively charged layer (3rd layer, charge density $\sim 0.003 \text{ e/nm}^3$) after which, charge neutrality develops (the 4th layer). The presence of the triple layer is essentially

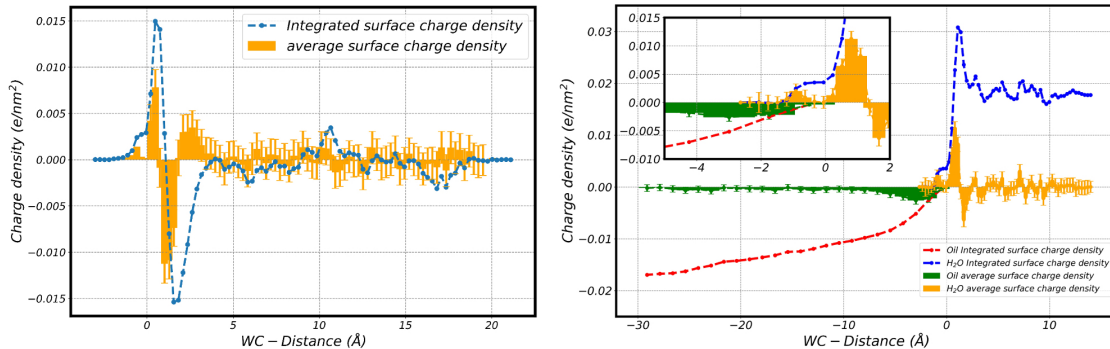


Figure 2: Charge density (yellow bars) and integrated surface charge density (blue line) obtained for the DDEC charges extracted from our calculations for the air-water (left panel) and oil-water (right panel) interfaces. For the oil phase in the right panel, the charge density is reported using green bars and the integrated surface charge density is shown by the red line. The inset in the right panel magnifies the charge oscillations right at the interface between the two phases.

caused by the asymmetry in the magnitude of the first two charged layers where the negative branch is about twice as large than that of its positive counterpart closer to the interface. The charge density shown, can be integrated from the vacuum to the bulk to give a better description of the cumulative surface charge. The dashed blue curve shows the integrated surface charge density - between 1-2Å from the WCI interface there is a substantial negative charge density of $\sim -0.015 e/nm^2$ which is about an order of magnitude larger than previous findings.^{24,25}

How does the behavior change near the oil-water interface? Rather unexpectedly, the oil phase is not a passive spectator in the charging mechanism. The right panel of Figure 2 shows similar distributions in charge density and integrated surface charge for both the water *and* the oil. As before, the zero on the x-axis corresponds to the position of the WCI surface. In stark contrast to the surface of water, there is a sharp peak of positive charge in the water phase just *below* the interface with a charge density of $\sim 0.07 e/nm^3$. This layer is followed by a negatively charge region of water with a lower charge density of $\sim 0.05 e/nm^3$. The complementary charge distributions of the dodecane molecules forms one of our central findings in this report namely that the oil phase is negatively charged. We observe a large

negative surface charge density of about -0.012 e/nm^2 in the oil phase. These results are striking since they show that there is a net charge transfer of ~ 0.4 electron charge from the water to the oil (Figure 1 SI). Furthermore, the magnitude of this surface charge is very similar to what is observed at the air-water interface, which is also consistent with the similarity in the zeta-potentials obtained from air and oil droplets.⁵⁸

Charging is Coupled to the Local Topology and Environment

In order to dissect the microscopic origins of the charge gradients observed at the interface, we turn next to examining how the charge is modulated by differences in topological defects. It is well appreciated, that fluctuations in liquid water both in the bulk²³ and at surface,⁵⁹ create local coordination defects which have asymmetries in the number of donated versus accepted hydrogen bonds. The bottom panel of Figure 1 depicts different types of water molecules that will form the focus of our discussion later ranging from the canonical tetrahedral waters that accept and donate two hydrogen bonds (2in-2out) to various other undercoordinated defects such as those that accept one/two and donate two/one hydrogen bonds (1in-2out and 2in-1out waters as described in the caption).

Using the four layers previously defined to describe the different charged layers, we determined how the relative concentration of different water molecules change as one moves from the interface to the bulk, as well as their relative contribution to the total charge. For clarity, the contributions to the total charge are given separately for the species that are positive or negative. In all the layers we show only the most dominant coordination states: for the first layer, this involves all species with a total population $> 0.5\%$, while for the other layers it is those that contribute at least 2% of the total population.

The 1st layer is dominated by many undercoordinated species due to the presence of the dangling O-H bonds.⁶⁰ Particularly relevant is the role of the 1in-0out and 2in-1out species both of which lead to a net positive contribution of charge within the first layer. It is also striking to note that in spite of being balanced in terms of hydrogen bonds, the 1in-1out

species noticeably contributes negatively to the overall charge underlining the importance that the asymmetry of hydrogen bonding itself does not exclusively control the charging behavior and that there are important collective polarization effects.

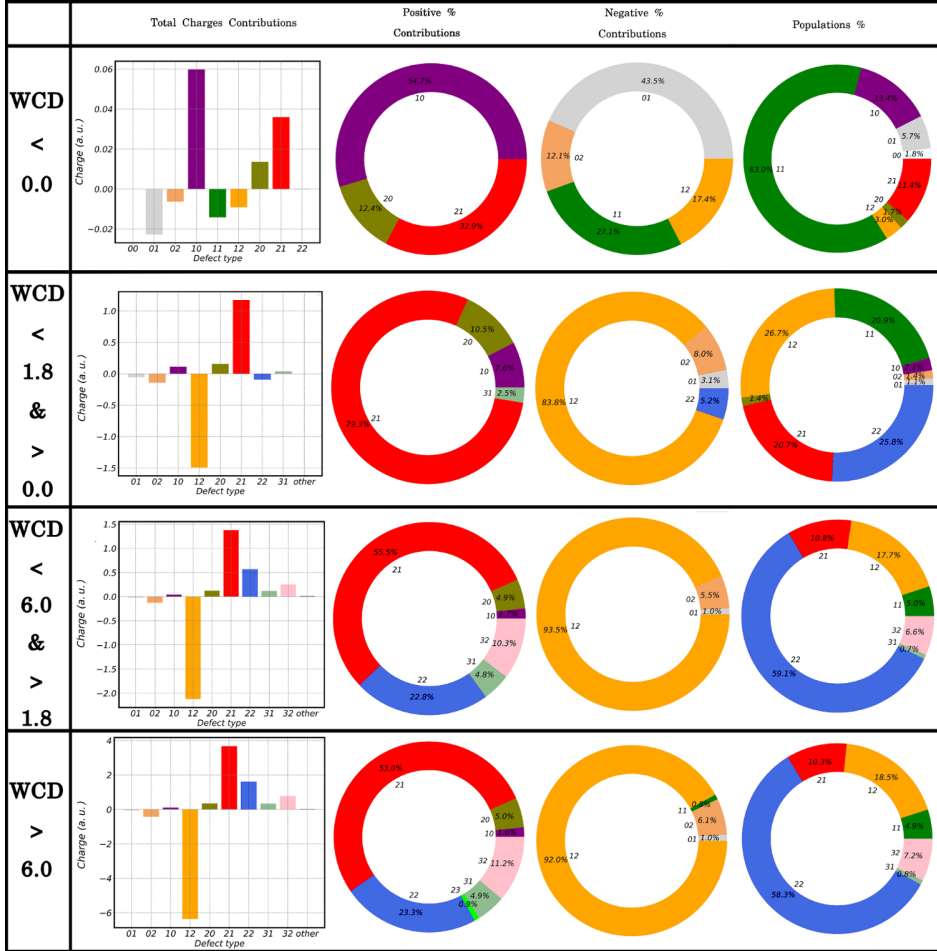


Figure 3: Analysis of the water-air interface layer-by-layer (as defined in the main text) in terms of the average total charge contribution, percentage contribution to the positive charge, percentage contribution to the negative charge and percentage contribution to the overall population for each water coordination configuration.

Layer two presents some drastic differences with respect to first and it is this region that provides important clues into the origin of the negative charge at the surface of water. The negative oscillation in charge between 0 and 1.8\AA below the WCI is dominated by the competition between the charging behavior of the 1in-2out and 2in-1out water molecules (second uppermost panel Figure 3). Contrary to what one might have expected, the behavior

is not symmetric. The total absolute charge of the 1in-2out waters is larger than 2in-1out by $\sim 0.3\ e$ (corresponding to a surface charge density of $-0.019\ e/nm^3$). Interestingly, this behavior is not exclusive to the interface but is a feature that continues to occur even in the bulk. Part of this effect originates from the fact that the concentration of 1in-2out waters is larger than 2in-1out waters consistent with previous studies²³ although the role of this difference in the creation of charge gradients has not been recognized until this point. Besides this, we will see later that charging behavior of the these two types of water defects are not symmetric across the region of the interface.

Despite its relatively lower weight, it is interesting to underline the negative contribution that the tetrahedral waters give to the total charge in the second layer. This behavior then swings in the opposite direction in the 3rd and 4th layers where the 2in-2out waters integrate to a net small positive charge. Similar to the traits of the 1in-1out water molecules right at the top of the surface of water, we find that the charge fluctuations are affected by other factors beyond the asymmetry in hydrogen bonding. In addition, what is also particularly important to observe as we move across different layers is that the dominant positive-negative branches of the 1in-2out and 2in-1out waters occur even in the bulk phase. Charge neutrality in bulk liquid water involves a complex mix of the 2in-2out, 3in-1out, 3in-2out and 2in-0out essentially counterbalancing the negative contribution of the 1in-2out water molecules that is not achieved by the 2in-1out defects.

Figure 3 provides a collective picture of the role of water-topology on charging but does not tell us anything about the nature of the fluctuations of individual molecules and how they are perturbed by the interface. In order to explicate this, we show in Figure 4 the charge distributions of the 2in-1out, 1in-2out, 2in-2out and 1in-0out water molecules in the four layers. These distributions confirm our intuitions built on the preceding analysis that the interfacial region agitates water molecules in subtle and very surprising ways. There is clearly a change in the average charge for water molecules in different layers. A more quantitative analysis of the differences can also be obtained by the first four moments reported in Figure

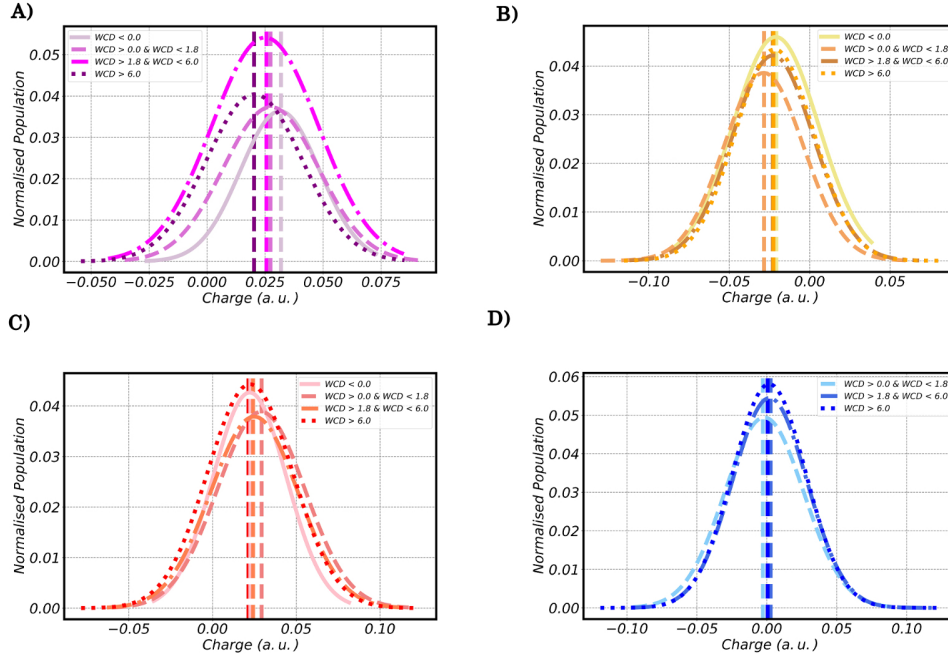


Figure 4: Layer-by-layer charge distributions of the 1in-out (panel A), 1in-2out (B), 2in-1out (C) and 2in-2out (D) water molecules for the water-air interface. The first moment is highlighted by a vertical line for each distribution.

2 of the Supporting Information. These results show that for the water-air interface the average charge on each water molecule for the 1in-2out, 2in-1out species increase from the 1st to the 2nd layer (right at the negative oscillation) just to decay again in the bulk like region. An increment of the average charge for the 1in-0out molecules is also observed at the surface. This increment, however, decreases monotonically moving into the bulk affirming the important role that this species has mainly for surface properties. As previously reported the tetrahedral coordinated waters in the 2nd layer are on average negatively charged and then regain a positive character towards the bulk. While the average charge changes between the 2nd and 3rd layer are moderate (~ 0.005 e on average) the huge increment in weight of the 2in-2out species between these two layers lead to sizeable changes in the overall charge contributions. This observation further solidifies the assumption that small variation in the average charge per molecules can lead to big changes in the interfacial system behaviour. These types of features would not be captured by models using a constant charge transfer

value^{24,25} that is not modulated by the local environment.

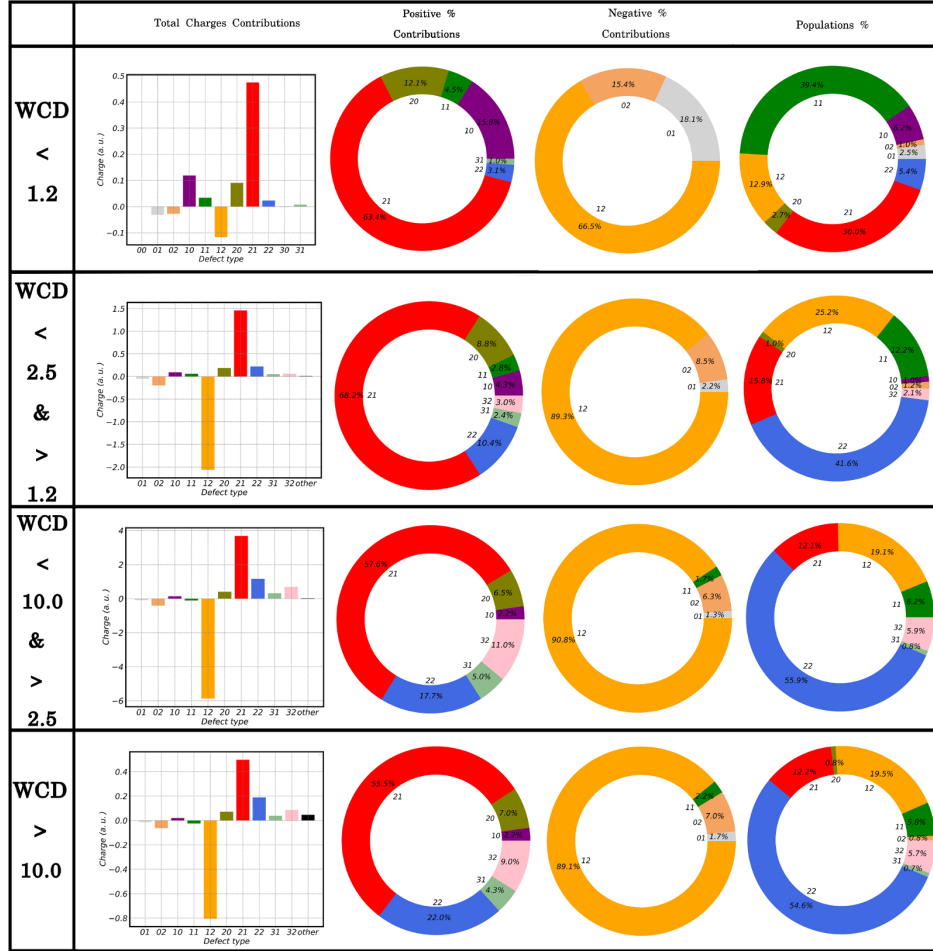


Figure 5: Analysis of the water-oil interface layer-by-layer (as defined in the main text) in terms of the average total charge contribution, percentage contribution to the positive charge, percentage contribution to the negative charge and percentage contribution to the overall population for each water coordination configuration.

Having understood the origins of the charge oscillations at the surface of water, we move next to examining how these properties behave near oil. In order to adequately compare the two interfaces we repeated the charge and population analysis previously done for the water-air system as a function of different layers (Figure 5) for the oil-water interface. The interfacial structure of water near the oil surface is quite different from that at the surface of water. The 1st layer is characterized by an increased presence of the 2in-1out coordination defects. In addition, the 1in-1out water molecules contribute positively to the overall charge.

These two effects conspire together to produce a much larger positive charge in the first layer compared to the surface of water. This is in essence activated by the transfer of charge to the oil phase. The 2nd layer derives very similar trends with respect to its air-water equivalent, except for the fact that in this case, the tetrahedral 2in-2out water integrate to a net positive charge. Beyond the 2nd layer, the behavior is very similar to that observed in Figure 3. Although the individual charge distributions for water near the oil show some differences (6 and Figure 2 SI, lower Table), the overall behavior is very similar -specifically, charge fluctuations of different water topologies and their sensitivity to proximity to the interface appears to be an important part of the physics of charging.

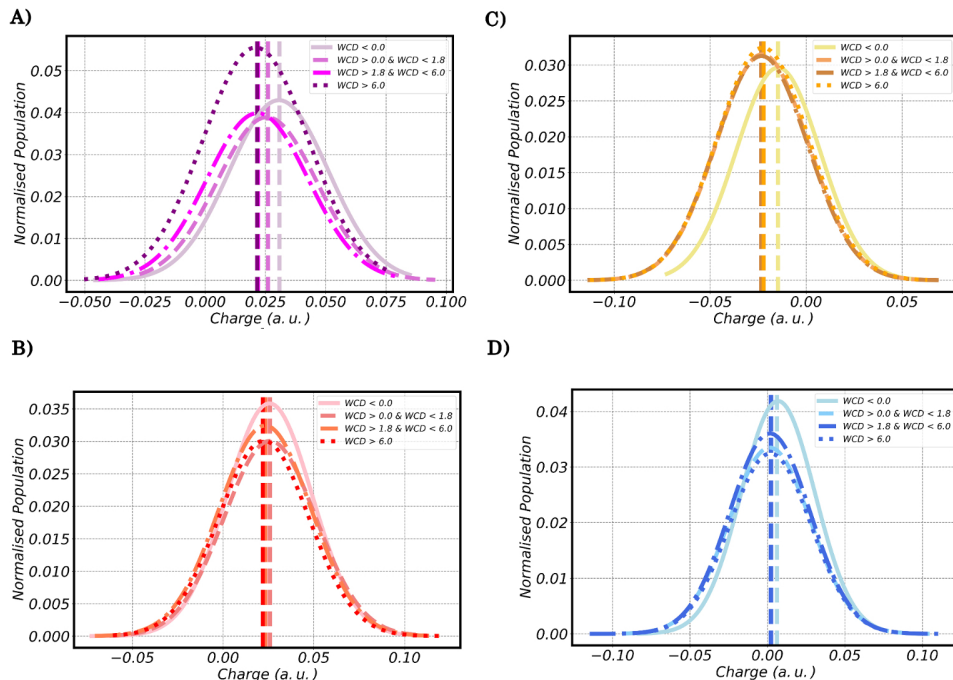


Figure 6: Layer-by-layer charge distributions of the 1in-out (panel A), 1in-2out (B), 2in-1out (C) and 2in-2out (D) water molecules for the water-oil interface. The first moment is highlighted by a vertical line for each distribution.

Figures 4 and 6 for the air and oil-water interfaces show that the charge on different water molecules sustains rather large fluctuations. Furthermore, the fact that tetrahedral waters can conspire to produce a positive total charge, suggests a highly non-trivial asymmetry in the charge transfer occurring on the donating versus accepting side of the hydrogen bond

network. Part of the origin of these asymmetries lie in the differences in the manner in which charge on water molecules is the fluctuations in the local tetrahedrality as seen in previous studies.⁶¹

The Role of Electronic Polarization and Charge Transfer

The stabilizing role of charge transfer between the hydrogen bonds of water molecules has been well appreciated in the literature.^{61,62} Its role however, at the surface of water and how it is modulated by defect fluctuations has not been recognized until this point. The situation near the oil-water interface is much more surprising and warrants a deeper examination.

In order to understand better the underlying quantum mechanical effects associated with the build up of surface charge, we performed an Energy Decomposition Analysis (EDA) as implemented in ONETEP.⁶³ The EDA analysis essentially provides a framework to disentangle various contributions of the interaction energy between the water and decane coming from electrostatics, polarization, exchange and charge transfer. The EDA analysis reported here was performed on approximately 60 clusters consisting of one decane molecule and all water molecules within 3.5 Å from it. The clusters were carved out from the thermal simulations described earlier and typically consist of about 12 H₂O molecules (see Figure 7A). For this subset of clusters, the average DDEC charge on the decane molecules was -0.056 e.

We begin by first showing the qualitative behavior involving the intra and inter-fragment electron reorganization in the clusters. Panels B and C of Figure 7 shows the electron density difference (EDD) surfaces that are obtained from the EDA calculations between intermediate states involving the extraction of the polarization (blue iso-surface) and charge transfer (yellow iso-surface) contributions (see Methods for more details). Interestingly, we observe that the polarization EDD mostly involves reorganization along the backbone carbon atoms of the decane. On the other hand, charge transfer appears as response of the electron density that is mainly localized on the hydrogen atoms of decane. In both cases, nearby water molecules also exhibit perturbations from both effects.

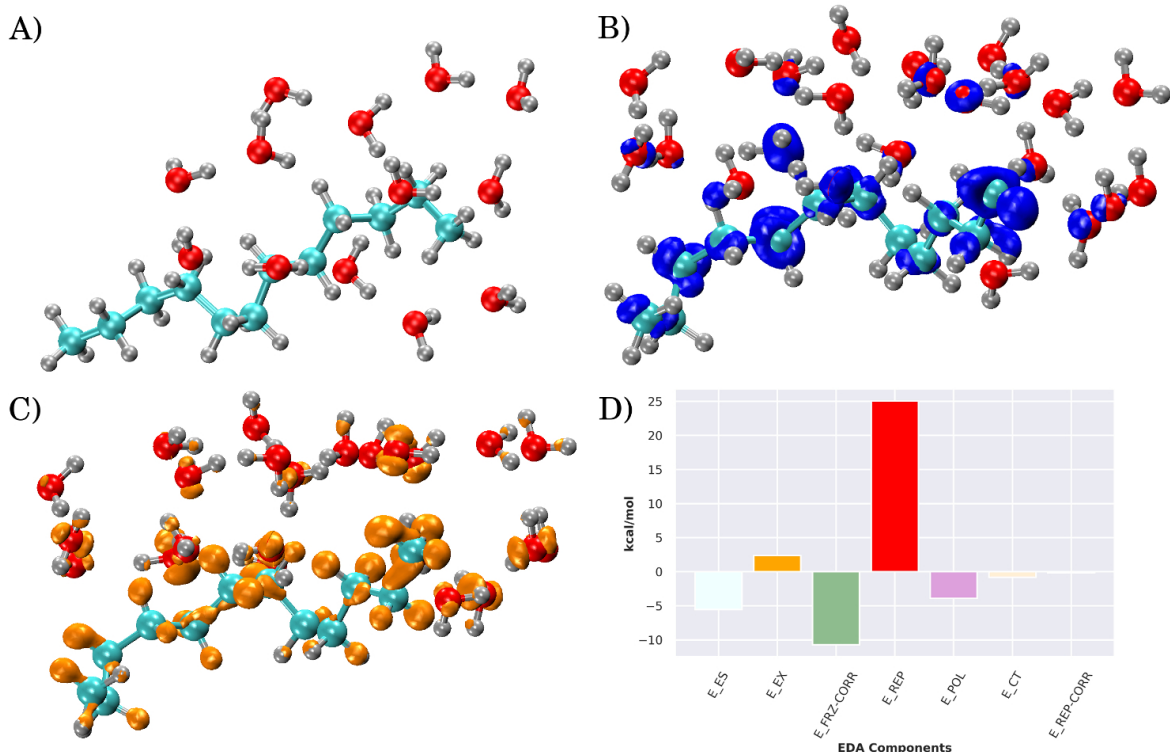


Figure 7: Sample representation of the clusters considered for the EDA calculations (Panel A). The Polarization (blue) and Charge Transfer (orange) Electron Density Difference for the same sample oil-water cluster are highlighted respectively in Panel B and C. The average energy component contributions calculated via EDA analysis for the 60 oil-water clusters are reported in Panel D. The acronyms of the different components are: E_{ES} is the Electrostatic Energy, E_{EX} is the Frozen Exchange Energy, $E_{FRZ-CORR}$ is the Frozen Correlation, E_{REP} is the Pauli-Repulsion Energy, E_{POL} is the (Stoll SCF-MI) Polarisation Energy, E_{CT} is the Charge Transfer Energy and $E_{REP-CORR}$ is the Repulsion Correlation.

A more quantitative measure of these effects at the oil-water interface can be explicated by examining the distributions associated with the various components of the interaction energy. Panel D of Figure 7 shows those components that are repulsive and attractive. The former are dominated by Pauli repulsion and exchange effects. On the other hand, charge transfer and polarization energetics contributes an attractive interaction that adds up to about 5 kcal/mol - for the clusters, this implies a binding energy of slightly under thermal energy per water molecule. As result of these charge transfer and polarization effects that render the oil phase negative and the water one positive the electrostatic component of the Energy is also attractive (~ 5 kcal/mol). Our findings in the previous section strongly suggest

that these effects are likely to be enhanced and also critical driving force in enhancing the negative surface charge observed at extended oil-water interfaces.

Discussion and Conclusions

The findings of our work give strong indication that different types of charge-transfer mechanisms can lead to a significant build up of surface charge density at hydrophobic interfaces. One of the essential ingredients associated with this phenomena, is the presence of local topological defects involving under-coordinated water molecules at the interface. These types of waters are most susceptible to asymmetries in the magnitude of charge transfer between the accepting and donating side which can leave them with a slight bias to take on either a positive or negative charge.

Near the surface of oil, something quite surprising happens: water defects can now inject some electron density into the oil phase leaving the latter negatively charged. The effective surface charge densities derived at the surface of oil is very similar to that near the air-water interface and is also in very good agreement with measurements from electrophoretic experiments. Lurking behind the link between the simulations and these experiments is the question of where the boundary of the slip plane should be placed in Figure 2.

Roke and co-workers proposed a qualitative mechanism (see Figure 5 of Ref. 26) for the effect of charge transfer on electrophoretic mobility. In this scenario, the slip plane resides several Angstroms from the oil surface and the role of fluctuations of water topologies is not considered. For the oil-water interface, our findings suggest that the slip plane will be pinned right near the oil droplet since it is negatively charged while the water in close proximity is positively charged. On the other hand for the air-bubbles, the slip plane must reside somewhere in between the boundary of the second and third charged layers (shown in the left panel of Figure 2).

A set of experiments that may also deserve another look at are surface sensitive photoelectron spectroscopy. Winter and Jungwirth combined both theory and experiments in a

series of papers to show that the valence band edge of sodium hydroxide solution could be used to interrogate the presence of hydroxide ions at the surface of water.⁶⁴ They found that the presence of the hydroxide ion could be identified by an enhancement in the states close to the valence band. Although it is beyond the scope of the current report, we examined the projected density of states (PDOS) on water molecules residing in the negatively charged layer at the surface of water and found that they contribute substantially to the valence band (see SI Figure 3,4 and 5). Qualitatively, the defects at the surface are about 0.5eV higher in energy than the mostly tetrahedral ones in the bulk (see SI Figure 3 upper-left panel) - this indicates an uncanny similarity between the anionic defect, the hydroxide ion, and defects in neutral water.

The mechanism associated with the response of the electronic degrees of freedom, as revealed by an energy decomposition analysis, involve a combination of both polarization and charge transfer. The coupling between the electronic reorganization and nuclear coordinates such as local topology, opens up some very interesting perspectives and questions for future lines of research. An obvious one centers around the generality of our results to other extended hydrophobic interfaces or more heterogeneous surfaces such as metal-oxides or even biological systems. In addition, the patchiness of surface charge at different interfaces deserves further investigation.³¹

Acknowledgement

EP and AH acknowledge the support from KAUST (Shaheen II project-k1263). EP and AH acknowledge Himashu Mishra for the useful discussions and insightful help provided during the work.

Supporting Information Available

The following files are available free of charge.

References

- (1) Hunter, R. J. *Zeta Potential in Colloid Science*; Elsevier, 1988.
- (2) Carruthers, J. C. The electrophoresis of certain hydrocarbons and their simple derivatives as a function of p. *Trans. Faraday Soc.* **1938**, *34*, 300–307.
- (3) Takahashi, M. Potential of Microbubbles in Aqueous Solutions: Electrical Properties of the Gas/Water Interface. *The Journal of Physical Chemistry B* **2005**, *109*, 21858–21864, PMID: 16853839.
- (4) Saykally, R. J. Two sides of the acid-base story. *Nature Chemistry* **2013**, *5*, 82 EP –.
- (5) Gray-Weale, A.; Beattie, J. K. An explanation for the charge on water's surface. *Phys. Chem. Chem. Phys.* **2009**, *11*, 10994–11005.
- (6) Beattie, J. K.; Djerdjev, A. M.; Warr, G. G. The surface of neat water is basic. *Faraday Discuss.* **2009**, *141*, 31–39.
- (7) Winter, B.; Faubel, M.; Vacha, R.; Jungwirth, P. Reply to comments on Frontiers Article Behavior of hydroxide at the water/vapor interface. *Chemical Physics Letters* **2009**, *481*, 19 – 21.
- (8) Mishra, H.; Enami, S.; Nielsen, R. J.; Stewart, L. A.; Hoffmann, M. R.; Goddard, W. A.; Colussi, A. J. Brønsted basicity of the air–water interface. *Proceedings of the National Academy of Sciences* **2012**, *109*, 18679–18683.
- (9) Petersen, P. B.; Saykally, R. J. Evidence for an Enhanced Hydronium Concentration at the Liquid Water Surface. *The Journal of Physical Chemistry B* **2005**, *109*, 7976–7980, PMID: 16851932.
- (10) Petersen, P. B.; Saykally, R. J. Is the liquid water surface basic or acidic? Macroscopic vs. molecular-scale investigations. *Chemical Physics Letters* **2008**, *458*, 255 – 261.

- (11) Tian, C.; Ji, N.; Waychunas, G. A.; Shen, Y. R. Interfacial Structures of Acidic and Basic Aqueous Solutions. *Journal of the American Chemical Society* **2008**, *130*, 13033–13039, PMID: 18774819.
- (12) Tarbuck, T. L.; Ota, S. T.; Richmond, G. L. Spectroscopic Studies of Solvated Hydrogen and Hydroxide Ions at Aqueous Surfaces. *Journal of the American Chemical Society* **2006**, *128*, 14519–14527, PMID: 17090035.
- (13) Gopalakrishnan, S.; Liu, D.; Allen, H. C.; Kuo, M.; Shultz, M. J. Vibrational Spectroscopic Studies of Aqueous Interfaces: Salts, Acids, Bases, and Nanodrops. *Chemical Reviews* **2006**, *106*, 1155–1175, PMID: 16608176.
- (14) Yan, X.; Delgado, M.; Aubry, J.; Gribelin, O.; Stocco, A.; Boisson-Da Cruz, F.; Bernard, J.; Ganachaud, F. Central Role of Bicarbonate Anions in Charging Water/Hydrophobic Interfaces. *The Journal of Physical Chemistry Letters* **2018**, *9*, 96–103, PMID: 29239612.
- (15) Okur, H. I.; Drexler, C. I.; Tyrode, E.; Cremer, P. S.; Roke, S. The Jones-Ray Effect Is Not Caused by Surface-Active Impurities. *The Journal of Physical Chemistry Letters* **2018**, *9*, 6739–6743, PMID: 30398354.
- (16) Buch, V.; Milet, A.; Vácha, R.; Jungwirth, P.; Devlin, J. P. Water surface is acidic. *Proceedings of the National Academy of Sciences* **2007**, *104*, 7342–7347.
- (17) Baer, M. D.; Kuo, I.-F. W.; Tobias, D. J.; Mundy, C. J. Toward a Unified Picture of the Water Self-Ions at the Air/Water Interface: A Density Functional Theory Perspective. *The Journal of Physical Chemistry B* **2014**, *118*, 8364–8372, PMID: 24762096.
- (18) Mundy, C. J.; Kuo, I.-F. W.; Tuckerman, M. E.; Lee, H.-S.; Tobias, D. J. Hydroxide anion at the air/water interface. *Chemical Physics Letters* **2009**, *481*, 2 – 8.

- (19) Petersen, M. K.; Iyengar, S. S.; Day, T. J. F.; Voth, G. A. The Hydrated Proton at the Water Liquid/Vapor Interface. *The Journal of Physical Chemistry B* **2004**, *108*, 14804–14806.
- (20) Tse, Y.-L. S.; Chen, C.; Lindberg, G. E.; Kumar, R.; Voth, G. A. Propensity of Hydrated Excess Protons and Hydroxide Anions for the AirWater Interface. *Journal of the American Chemical Society* **2015**, *137*, 12610–12616, PMID: 26366480.
- (21) Kumar, R.; Knight, C.; Voth, G. A. Exploring the behaviour of the hydrated excess proton at hydrophobic interfaces. *Faraday Discuss.* **2013**, *167*, 263–278.
- (22) Mamatkulov, S. I.; Allolio, C.; Netz, R. R.; Bonthuis, D. J. Orientation-Induced Adsorption of Hydrated Protons at the AirWater Interface. *Angewandte Chemie International Edition* **2017**, *56*, 15846–15851.
- (23) Gasparotto, P.; Hassanali, A. A.; Ceriotti, M. Probing Defects and Correlations in the Hydrogen-Bond Network of ab Initio Water. *Journal of Chemical Theory and Computation* **2016**, *12*, 1953–1964, PMID: 26881726.
- (24) Vcha, R.; Marsalek, O.; Willard, A. P.; Bonthuis, D. J.; Netz, R. R.; Jungwirth, P. Charge Transfer between Water Molecules As the Possible Origin of the Observed Charging at the Surface of Pure Water. *The Journal of Physical Chemistry Letters* **2012**, *3*, 107–111.
- (25) Wick, C. D.; Lee, A. J.; Rick, S. W. How intermolecular charge transfer influences the air-water interface. *The Journal of Chemical Physics* **2012**, *137*, 154701.
- (26) Samson, J.-S.; Scheu, R.; Smolentsev, N.; Rick, S. W.; Roke, S. Sum frequency spectroscopy of the hydrophobic nanodroplet/water interface: Absence of hydroxyl ion and dangling OH bond signatures. *Chemical Physics Letters* **2014**, *615*, 124 – 131.

- (27) Bjørneholm, O.; Hansen, M. H.; Hodgson, A.; Liu, L.-M.; Limmer, D. T.; Michaelides, A.; Pedevilla, P.; Rossmeis, J.; Shen, H.; Tocci, G.; Tyrode, E.; Walz, M.-M.; Werner, J.; Bluhm, H. Water at Interfaces. *Chemical Reviews* **2016**, *116*, 7698–7726, PMID: 27232062.
- (28) Griffith, E. C.; Vaida, V. In situ observation of peptide bond formation at the water–air interface. *Proceedings of the National Academy of Sciences* **2012**, *109*, 15697–15701.
- (29) Mompeán, C.; Marín-Yaseli, M. R.; Espigares, P.; González-Toril, E.; Zorzano, M.-P.; Ruiz-Bermejo, M. Prebiotic chemistry in neutral/reduced-alkaline gas-liquid interfaces. *Scientific Reports* **2019**, *9*, 1916.
- (30) Lin, Z.-H.; Cheng, G.; Lin, L.; Lee, S.; Wang, Z. L. Water/Solid Surface Contact Electrification and its Use for Harvesting Liquid-Wave Energy. *Angewandte Chemie* **2013**, *125*, 12777–12781.
- (31) Baytekin, H. T.; Patashinski, A. Z.; Branicki, M.; Baytekin, B.; Soh, S.; Grzybowski, B. A. The Mosaic of Surface Charge in Contact Electrification. *Science* **2011**, *333*, 308–312.
- (32) Abraham, M. J.; Murtola, T.; Schulz, R.; Páll, S.; Smith, J. C.; Hess, B.; Lindahl, E. GROMACS: High performance molecular simulations through multi-level parallelism from laptops to supercomputers. *SoftwareX* **2015**, *1-2*, 19 – 25.
- (33) Abascal, J. L. F.; Vega, C. A general purpose model for the condensed phases of water: TIP4P/2005. *The Journal of Chemical Physics* **2005**, *123*, 234505.
- (34) Siu, S. W. I.; Pluhackova, K.; Bockmann, R. A. Optimization of the OPLS-AA Force Field for Long Hydrocarbons. *Journal of Chemical Theory and Computation* **2012**, *8*, 1459–1470, PMID: 26596756.

- (35) Parrinello, M.; Rahman, A. Polymorphic transitions in single crystals: A new molecular dynamics method. *Journal of Applied Physics* **1981**, *52*, 7182–7190.
- (36) Alejandre, J.; Chapela, G. A. The surface tension of TIP4P/2005 water model using the Ewald sums for the dispersion interactions. *The Journal of Chemical Physics* **2010**, *132*, 014701.
- (37) Skylaris, C.-K.; Haynes, P. D.; Mostofi, A. A.; Payne, M. C. Introducing ONETEP: Linear-scaling density functional simulations on parallel computers. *The Journal of Chemical Physics* **2005**, *122*, 084119.
- (38) Bowler, D. R.; Miyazaki, T. $\mathcal{O}(N)$ methods in electronic structure calculations. *Reports on Progress in Physics* **2012**, *75*, 036503.
- (39) Prodan, E.; Kohn, W. Nearsightedness of electronic matter. *Proceedings of the National Academy of Sciences of the United States of America* **2005**, *102*, 11635–11638.
- (40) Cloizeaux, J. D. Energy Bands and Projection Operators in a Crystal: Analytic and Asymptotic Properties. *Phys. Rev.* **1964**, *135*, A685–A697.
- (41) Ismail-Beigi, S.; Arias, T. A. Locality of the Density Matrix in Metals, Semiconductors, and Insulators. *Phys. Rev. Lett.* **1999**, *82*, 2127–2130.
- (42) McWeeny, R. Some Recent Advances in Density Matrix Theory. *Rev. Mod. Phys.* **1960**, *32*, 335–369.
- (43) Hernandez, E.; Gillan, M. J. Self-consistent first-principles technique with linear scaling. *Phys. Rev. B* **1995**, *51*, 10157–10160.
- (44) Skylaris, C.-K.; Mostofi, A. A.; Haynes, P. D.; Diéguez, O.; Payne, M. C. Nonorthogonal generalized Wannier function pseudopotential plane-wave method. *Phys. Rev. B* **2002**, *66*, 035119.

- (45) He, L.; Vanderbilt, D. Exponential Decay Properties of Wannier Functions and Related Quantities. *Phys. Rev. Lett.* **2001**, *86*, 5341–5344.
- (46) VandeVondele, J.; Krack, M.; Mohamed, F.; Parrinello, M.; Chassaing, T.; Hutter, J. Quickstep: Fast and accurate density functional calculations using a mixed Gaussian and plane waves approach. *Computer Physics Communications* **2005**, *167*, 103 – 128.
- (47) Becke, A. D. Density-functional exchange-energy approximation with correct asymptotic behavior. *Phys. Rev. A* **1988**, *38*, 3098–3100.
- (48) Lee, C.; Yang, W.; Parr, R. G. Development of the Colle-Salvetti correlation-energy formula into a functional of the electron density. *Phys. Rev. B* **1988**, *37*, 785–789.
- (49) Grimme, S. Semiempirical GGA-type density functional constructed with a long-range dispersion correction. *Journal of Computational Chemistry* **2006**, *27*, 1787–1799.
- (50) Kleinman, L.; Bylander, D. M. Efficacious Form for Model Pseudopotentials. *Phys. Rev. Lett.* **1982**, *48*, 1425–1428.
- (51) <http://opium.sourceforge.net/sci.html>.
- (52) Manz, T. A.; Sholl, D. S. Improved Atoms-in-Molecule Charge Partitioning Functional for Simultaneously Reproducing the Electrostatic Potential and Chemical States in Periodic and Nonperiodic Materials. *Journal of Chemical Theory and Computation* **2012**, *8*, 2844–2867, PMID: 26592125.
- (53) Lee, L. P.; Limas, N. G.; Cole, D. J.; Payne, M. C.; Skylaris, C.-K.; Manz, T. A. Expanding the Scope of Density Derived Electrostatic and Chemical Charge Partitioning to Thousands of Atoms. *Journal of Chemical Theory and Computation* **2014**, *10*, 5377–5390, PMID: 26583221.
- (54) Becke, A. D. Densityfunctional thermochemistry. III. The role of exact exchange. *The Journal of Chemical Physics* **1993**, *98*, 5648–5652.

- (55) Møller, C.; Plesset, M. S. Note on an Approximation Treatment for Many-Electron Systems. *Phys. Rev.* **1934**, *46*, 618–622.
- (56) Babin, V.; Leforestier, C.; Paesani, F. Development of a First Principles Water Potential with Flexible Monomers: Dimer Potential Energy Surface, VRT Spectrum, and Second Virial Coefficient. *Journal of Chemical Theory and Computation* **2013**, *9*, 5395–5403, PMID: 26592277.
- (57) Willard, A. P.; Chandler, D. Instantaneous Liquid Interfaces. *The Journal of Physical Chemistry B* **2010**, *114*, 1954–1958.
- (58) Agmon, N.; Bakker, H. J.; Campen, R. K.; Henchman, R. H.; Pohl, P.; Roke, S.; Thmer, M.; Hassanali, A. Protons and Hydroxide Ions in Aqueous Systems. *Chemical Reviews* **2016**, *116*, 7642–7672, PMID: 27314430.
- (59) Giberti, F.; Hassanali, A. A. The excess proton at the air-water interface: The role of instantaneous liquid interfaces. *The Journal of Chemical Physics* **2017**, *146*, 244703.
- (60) Hsieh, C.-S.; Campen, R. K.; Vila Verde, A. C.; Bolhuis, P.; Nienhuys, H.-K.; Bonn, M. Ultrafast Reorientation of Dangling OH Groups at the Air-Water Interface Using Femtosecond Vibrational Spectroscopy. *Phys. Rev. Lett.* **2011**, *107*, 116102.
- (61) Kühne, T. D.; Khaliullin, R. Z. Electronic signature of the instantaneous asymmetry in the first coordination shell of liquid water. *Nature Communications* **2013**, *4*, 1450 EP –, Article.
- (62) Khaliullin, R.; Bell, A.; Head-Gordon, M. Electron Donation in the WaterWater Hydrogen Bond. *Chemistry A European Journal* **2009**, *15*, 851–855.
- (63) Phipps, M. J. S.; Fox, T.; Tautermann, C. S.; Skylaris, C.-K. Intuitive Density Functional Theory-Based Energy Decomposition Analysis for ProteinLigand Interactions. *Journal of Chemical Theory and Computation* **2017**, *13*, 1837–1850.

- (64) Winter, B.; Faubel, M.; Vcha, R.; Jungwirth, P. Behavior of hydroxide at the water/vapor interface. *Chemical Physics Letters* **2009**, *474*, 241 – 247.